



Available online at www.sciencedirect.com

ScienceDirect



Nuclear Physics A 1024 (2022) 122475

www.elsevier.com/locate/nuclphysa

Conserved number fluctuations in interacting hadron resonance gas model

S.P. Behera*, D.K. Mishra

Nuclear Physics Division, Bhabha Atomic Research Center, Mumbai 400085, India

Received 9 February 2022; received in revised form 11 May 2022; accepted 11 May 2022

Available online 17 May 2022

Abstract

Fluctuations of net-baryon, net-charge and net-strangeness numbers are studied within the framework of ideal hadron resonance gas (IHRG), including attractive and repulsive van der Waals interactions. The binding energy and thermodynamic parameters are calculated for different extended versions of the HRG (E-HRG) model. The susceptibility ratios of conserved numbers are estimated in full phase-space using various HRG models that show a strong dependence on collision energies. The effect of kinematic cuts (transverse momentum (p_T) and pseudo-rapidity (η)) on those ratios of conserved numbers are also discussed. It is observed that, the normalized susceptibility ratios as a function of collision energies strongly depend on lower p_T cut-off and $\Delta \eta$ window. The E-HRG models are very sensitive to kinematic acceptance even for net-proton fluctuations. The susceptibility ratios calculated from different HRG models with proper kinematic acceptances are compared with the experimental measurements, which will help to better understand the phase transition and existence of critical point in the QCD phase diagram. © 2022 Elsevier B.V. All rights reserved.

Keywords: Hadron resonance gas; Van-der Waals; Excluded volume; Thermodynamic parameters

1. Introduction

One of the major goals of the high-energy heavy-ion collisions is to study the structure of quantum chromodynamics (QCD) phase diagram at finite temperature (T) and baryon chemical

E-mail addresses: shiba@barc.gov.in (S.P. Behera), dkmishra@barc.gov.in (D.K. Mishra).

^{*} Corresponding author.

potential (μ_B) [1]. It is a well-known fact that the first-order liquid-gas phase transition takes place in a system consists of atoms and/or molecules, interacting nucleons, and also expected between hadrons and quark-gluon plasma (QGP) at large μ_B . Lattice QCD calculations suggest a smooth cross over from hadronic to QGP phase in the temperature range of 150–190 MeV at $\mu_B \simeq 0$ [2,3]. Several other models predict a first-order phase transition at large μ_B and small T [4,5]. Hence, there should be a point at which the first-order phase transition ends in the $T-\mu_B$ plane named as the critical end point (CEP) [6–8]. At lower temperature $T \sim 100$ –150 MeV, the lattice QCD calculations exhibit similar feature to observables calculated using non-interacting (ideal) hadron resonance gas (IHRG) model. The disagreement between lattice QCD and IHRG at higher temperature T > 160 MeV attributes to quickly melting of hadrons [9–11].

In recent years, lots of effort have been made on both theoretical and experimental fronts to study the QCD critical point using fluctuations of conserved quantities. It has been suggested that the energy dependence of conserved numbers like net-baryon, net-charge, and net-strangeness fluctuations should show a non-monotonic behavior, as a possible signature of CEP [12–14]. Experimentally, the location of the CEP can be explored by varying the center-of-mass energy $(\sqrt{s_{NN}})$ of the colliding ions [12,13] and studying various thermodynamic parameters. The beam energy scan program performed at Relativistic Heavy-Ion Collider (RHIC) is motivated to investigate the location of CEP using the fluctuations of net-proton [15–17], net-charge [18,19] and net-kaon [20] multiplicities at various collision energy. Several other experiments such as the HADES experiment at GSI, NA61-SHINE experiment at CERN-SPS energies are being carried out to investigate the medium formed at large baryon chemical potential. In future Compressed Baryonic Matter (CBM) experiment at FAIR, GSI and the Nuclotron-based Ion Collider fAcility (NICA) at JINR, Dubna are planned to study the nuclear matter at large baryon chemical potential.

The hadron resonance gas (HRG) model has been very successful to explain the particle multiplicities measured from the experimental data in high-energy heavy-ion collisions typical Alternating Gradient Synchrotron (AGS) at BNL to those of the Large Hadron Collider (LHC) energies [21–23]. It is argued that the attractive interactions between hadrons are taken into account by the presence of all known resonance states in the thermal system. Several E-HRG model including the attractive and repulsive interactions between hadrons have been widely discussed [24–31]. It is a well known fact that both the long-range attraction as well as the short-range repulsion are important to describe the strongly interacting matter [31,32].

The excluded volume hadron resonance gas (EVHRG) model is one of them in which the effect of repulsive interaction between the hadrons at short distances are introduced [27,28]. The difference between EVHRG and IHRG is governed by the radius parameter used for the hadrons. The electromagnetic charge radii of hadrons have been reported by various groups [33–37]. Earlier radii values of 0.62 and 0.8 fm for meson and baryon, respectively are considered to explain the particle yields at AGS and SPS energies [25]. Further, a more realistic approach has been considered to incorporate the repulsive behavior of the nucleus-nucleus potential using a hard-core radius (~ 0.3 fm) for both mesons and baryons as obtained from nucleon-nucleon scattering [38]. Several recent studies have also used different radii of 0.2–0.3 fm for meson and baryon to calculate the net-proton fluctuations [10,28,29].

Taking the flavor dependent hard-core radius in the EVHRG model, a better agreement with the experimental yield at LHC energy is observed [39]. In this model, an inverse mass-volume relation is employed for strange particles to explain the particle yields for nucleus-nucleus collisions at LHC energy [39]. The description of particle yield improves at lower collision energies up to LHC energy by considering a bag-like parameterization for the eigenvolume [40,41].

Further, the EVHRG equation of state has also been used for the hydrodynamical models of nucleus-nucleus collision [42,43]. The lattice QCD calculations also indicate a presence of corrections for the finite size of hadrons [26].

The long-range attractive interaction in the HRG model is introduced by considering van der Waals (VDW) type nucleon-nucleon interaction. Recently, such interaction with the HRG (VDWHRG) model has been studied taking both attractive and repulsive interactions [10,44, 45]. The VDWHRG model shows a first-order liquid-gas phase transition in nuclear matter at small temperature and large μ_B , which is absent in IHRG or EVHRG models. In Ref. [44], the VDW parameters a (attractive) and b (repulsive) are fixed to reproduce the properties of nuclear matter in its ground state, i.e. number density $n = n_0 = 0.16$ fm⁻³ and binding energy per nucleon E/A = -16 MeV. With these conditions, the resulting VDW parameters are obtained as; $a \simeq 329 \text{ MeV fm}^3$ and $b = 3.42 \text{ fm}^3$. Note that particle volume parameter b is connected to the hard-core radius as $r = [3b/(16\pi)]^{1/3} \simeq 0.59$ fm. These values of a and b are used in the VDWHRG model which predicts a liquid-gas first-order phase transition in the nuclear matter with a critical point at $T_c \simeq 19.7$ MeV and $\mu_B \simeq 908$ MeV [45]. Further, it is shown that using the normal nuclear matter VDW parameters a and b, the VDWHRG model and lattice QCD results on fluctuations and correlations of conserved charges resemble in the crossover region at zero chemical potential [10]. Another recent study in Ref. [33] reported the VDW parameters as $a = 1250 \text{ MeV fm}^3$ and $b = 5.747 \text{ fm}^3$, observed a phase transition in the VDWHRG model at large chemical potential with a critical point at T = 62.1 MeV and $\mu_B = 708$ MeV in the $T - \mu_B$ phase diagram.

In the present study, we discuss different extended versions of the HRG (E-HRG) model as listed in Table 1, and calculate the observables in terms of susceptibility ratios for the conserved number fluctuations. These models use different values of hard-core radii of the hadrons which are as follows: ideal HRG without interaction (IHRG) [46,47], with fixed values of hard-core radii of mesons and baryons (EVHRG) [29,31], with flavor dependent radii of hadrons (FLEVHRG) [39], with different values of VDW parameters (VDWHRG1 [10] and VDWHRG2 [33]). These models have been used to explain the thermal properties [29–31], fluctuation observables [10], and criticality [33] of the QCD matter. The excluded volume models EVHRG and FLEVHRG better describe the particle yields as compared to IHRG. Further, models based on VDW interactions VDWHRG1 and VDWHRG2 predict a critical point in the $T - \mu_B$ phase diagram. In the present study, we investigate which of the above models best describe the experimental data on higher moments of conserved numbers. In the present model, we have not considered global conservation into account. As discussed in Ref. [48], baryon number conservation results in a substantial effect on the higher order fluctuations. However, the effect of global conservation of charges depends on the fraction of charges measured in the detector acceptance, which is found to be small within the experimental acceptance discussed in this paper.

The paper is organized as follows: In the following section, various extensions to the ideal HRG such as EVHRG and VDWHRG models are discussed. In Sec. 3 the results on thermodynamic parameters and susceptibility ratios obtained from different models are presented. The effect of pseudo-rapidity acceptance, lower transverse momentum selection threshold and comparison with the experimental results are also described in Sec. 3. Finally, in Sec. 4, we summarize our findings and discuss the implications of this work.

Case	Name	a (MeV fm ³)	b (fm ³)	r (fm)
I	IHRG [46,47]	0	0	0
II	EVHRG [29,31]	0	0.134 (meson), 0.452 (baryon)	0.2 (meson), 0.3 (baryon)
III	FLEVHRG [39]	0	αm (non-strange)	$[3\alpha m/(16\pi)]^{1/3}$ (non-strange)
			γ/m (strange)	$[3\gamma/(16\pi m)]^{1/3}$ (strange)
			$\alpha = 2.1 \text{ fm}^3/\text{GeV}, \gamma = 1.38 \text{ fm}^3$.	GeV
IV	VDWHRG1 [10]	329	3.42	0.588
V	VDWHRG2 [33]	1250	5.747	0.7

Table 1
List of van der Waals parameters used for the different extended versions of HRG model calculations.

2. Model description

Several studies are performed using HRG model and its extended versions [46,47,49–53]. Out of different extensions of the IHRG models, here we discuss two of them. The first one is the excluded volume HRG model (EVHRG) in which the effects of hadron repulsion at short distances are accounted and the other one with van der Waals (VDWHRG) type in which both attractive and repulsive interactions are considered. In the following subsections, we will briefly discuss each version of the model.

2.1. Ideal hadron resonance gas (IHRG) model

In an ideal HRG model, the partition function includes all relevant degrees of freedom of the confined, strongly interacting matter and consists of point-like hadrons and resonances [46]. The heavy-ion experiments cover a limited phase space, one can access only a part of the fireball produced in the collision which resembles the grand canonical ensemble (GCE) [47,54]. Assuming a thermal system produced in the heavy-ion collisions, the thermodynamic pressure P in the GCE can be written as a sum of the partial pressures of all the particle species i:

$$P/T^4 = \frac{1}{T^4} \sum_{i} P_i^{id}(T, V, \mu_i) = \frac{1}{VT^3} \sum_{i} \ln Z_i^{id}$$
 (1)

where *i* corresponds to either baryons (B) or mesons (M), V is the volume of the system and T is the temperature. The grand canonical partition function (Z_i) of *i*th particle can be written as

$$\ln Z_i^{id}(T, V, \mu_i) = \pm \frac{Vg_i}{2\pi^2} \int p^2 dp \ln\{1 \pm \exp[(\mu_i - E)/T]\},\tag{2}$$

where g_i is the degeneracy factor and μ_i is the chemical potential. The total chemical potential of the individual particle is $\mu_i = B_i \mu_B + Q_i \mu_Q + S_i \mu_S$, where B_i , Q_i and S_i are the baryon, electric-charge and strangeness number of the *i*th particle, with corresponding chemical potentials μ_B , μ_Q and μ_S , respectively. The +ve and -ve signs correspond to baryons and mesons, respectively. In this calculation, all the mesons and baryons of mass upto 2.5 GeV as listed in the particle data book are considered. The volume element (d^3p) of a particle of mass m can be written as $d^3p = p_Tm_T \cosh \eta \ dp_T \ d\eta \ d\phi$ and energy $E = m_T \cosh \eta$, where m_T is the transverse mass $= \sqrt{m^2 + p_T^2}$ with p_T , η and ϕ represent the transverse momentum, pseudo-rapidity, and azimuthal angle, respectively. Thermodynamic variables for the quantum ideal gas such as

the pressure (P^{id}) , the energy density (ε^{id}) , the particle number density (n^{id}) , and the entropy density s^{id} are given by;

$$P^{id} = \sum_{i} P_{i}^{id}$$

$$= \sum_{i} \pm \frac{g_{i}T}{2\pi^{2}} \int_{-\infty}^{\infty} p^{2} dp \ln\{1 \pm \exp[(\mu_{i} - E)/T]\}$$
(3)

$$n^{id} = \sum_{i} \frac{g_i}{2\pi^2} \int_{0}^{\infty} \frac{p^2 dp}{\exp[(E_i - \mu_i)/T] \pm 1}$$
 (4)

$$\varepsilon^{id} = \sum_{i} \frac{g_i}{2\pi^2} \int_{0}^{\infty} \frac{p^2 dp}{\exp[(E_i - \mu_i)/T] \pm 1} E_i \tag{5}$$

$$s^{id} = \sum_{i} \pm \frac{g_{i}}{2\pi^{2}} \int_{0}^{\infty} p^{2} dp \left[\ln \left(1 \pm \exp\left(-\frac{(E_{i} - \mu_{i})}{T} \right) \right) \right]$$

$$\pm \frac{(E_{i} - \mu_{i})}{T \left\{ \exp\left[(E_{i} - \mu_{i})/T \right] \pm 1 \right\}}$$
(6)

In the IHRG model, all the particles are in equilibrium at the time of chemical freeze-out. In order to compare the thermodynamic quantities and the susceptibility ratios calculated from the IHRG model with the experimental observables, it is essential to have the beam energy dependence of freeze-out parameters (μ_B and T_f). The parameterized form of freeze-out parameters T_f and μ_B as a function of $\sqrt{s_{NN}}$ are used as given in Ref. [22]. The energy dependence of μ_B is given as, $\mu_B(\sqrt{s_{NN}}) = 1.308/(1 + 0.273\sqrt{s_{NN}})$ and the μ_B dependence of freeze-out temperature is given as $T_f(\mu_B) = 0.166 - 0.139\mu_B^2 - 0.053\mu_B^4$. Further, the energy dependence of μ_Q and μ_S are parameterized as given in Ref. [46]. The freeze-out parameters are found to be same in case of IHRG and EVHRG within small uncertainties as mentioned in Ref. [29]. We have used the above freeze-out parameterization for T_f and μ_B) in the EVHRG and VDWHRG models, although the μ_B will be replaced with reduced chemical potential as discussed in the following section.

2.2. HRG model with repulsive interaction (EVHRG)

In this section, the role of repulsive interactions within hadrons which lead to the excluded volume HRG model (EVHRG) is described. The repulsive interactions are required, particularly at very high T and/or at large μ_B , to see the qualitative features of strong interactions where the ideal gas assumption becomes inadequate. In contrast to HRG, the geometrical size of the hadrons are incorporated explicitly in the EVHRG model. In this model the system volume V is replaced by available volume V_{av} , which approximates the short-range repulsive interaction between hadrons [26–29,31]

$$V \to V_{av} = V - \sum_{i} b_i N_i \tag{7}$$

where N_i is the particle number and $b_i = \frac{16}{3}\pi r_i^3$ is the excluded volume of the *i*th particle with hard-core radius r_i . In grand canonical ensemble, with the reduced volume correction leads to the transcendental equation for the pressure, can be written as [27]

$$P^{ev}(T,\mu) = \sum_{i} P_i^{id}(T,\tilde{\mu}_i), \tag{8}$$

where the reduced chemical potential for the ith particle is

$$\tilde{\mu_i} = \mu_i - b_i P(T, \mu_i) \tag{9}$$

The other thermodynamic quantities are expressed as

$$n_i = n_i(T, \mu_i) = \frac{\partial P}{\partial \mu_i} = \frac{n_i^{id}(T, \tilde{\mu}_i)}{1 + \sum_i b n_i^{id}(T, \tilde{\mu}_i)},\tag{10}$$

$$\varepsilon = \frac{\sum_{i} \varepsilon_{i}^{id}(T, \tilde{\mu_{i}})}{1 + \sum_{i} b_{i} n_{i}^{id}(T, \tilde{\mu_{i}})},\tag{11}$$

$$s = \frac{\sum_{i} s_{i}^{id}(T, \tilde{\mu_{i}})}{1 + \sum_{i} b_{i} n_{i}^{id}(T, \tilde{\mu_{i}})}$$
(12)

The values of above thermodynamic quantities on the left hand side are lower as compared to the same obtained from IHRG due to the suppression factor $[1+\sum_i b_i n_i^{id}(T,\tilde{\mu_i})]$ in the denominator and also due to the reduced chemical potential $\mu_i \to \tilde{\mu_i}$. In case of constant volume b_i for all the considered particle species, the overall suppression of each hadron density n_i due to the excluded volume effects as compared to their ideal gas values n_i^{id} is essentially the same. A small difference arises due to the quantum-statistical effects. Therefore, the particle number ratios are almost unchanged, and rescaling the total volume V, one may then obtain the average yield $\langle N \rangle$ values equal to those in the IHRG. If the b_i s are chosen to be different for different particles, the suppression will be stronger for particles having larger hard-core radius [29,40]. The chemical freeze-out parameters T and μ_B estimated in EVHRG by fitting to data on hadron multiplicities are identical to those obtained within the IHRG model [29]. This leads to a misconception that the inclusion of the eigenvolume interactions into the HRG has a negligible effect on the thermal fits. However, the reduced chemical potential $\tilde{\mu}_i$ is different in EVHRG as compared to the IHRG model.

The above EVHRG model discussion has been carried out considering fixed radii for mesons and baryons. However, the recent study by taking flavor dependent eigenvolume in the EVHRG model, the mean hadron multiplicities measured in central Pb+Pb collisions at LHC energy are better explained [39]. In such a case, the bag model with linear mass-volume relation for non-strange particles are used as $b_i = \alpha m_i$, i.e. hard-core radius $r_i = [3\alpha m_i/(16\pi)]^{1/3}$ fm and for strange particles $b_i = \gamma/m_i$, i.e $r_i = [3\gamma/(16\pi m_i)]^{1/3}$ fm. Where parameters $\alpha = 2.1$ fm³/GeV and $\gamma = 1.38$ fm³ GeV are fixed by specifying the proton radius and Λ radius, respectively [39].

2.3. HRG model with attractive and repulsive interaction (VDWHRG)

The interactions between nucleon-nucleon are not included in the IHRG model, hence this model is not able to explain the properties of nuclear matter at large baryon densities and lower temperatures. However, by considering the interactions among nucleons, it has been predicted that the VDW model shows the first-order liquid-gas phase transition which ends at the critical

point [10]. A similar feature is also expected for the QCD phase diagram. With this model, the basic features of nuclear matter have been successfully described by the VDW equation with Fermi statistics. In the canonical ensemble the pressure P(T, n) of the VDW equation can be written as

$$P(T,n) = \frac{NT}{V - hN} - a\frac{N^2}{V^2} = \frac{nT}{1 - hn} - an^2$$
 (13)

where N is the number of particles and n = N/V is the number density. The parameters a and b describe the attractive and repulsive interactions, respectively and both are positive. The first term of Eq. (13) represents the excluded volume correction part as described in Sec. 2.2. For a = 0, Eq. (13) reduces to EVHRG model, where only repulsive part is included. For both a and b are equal to zero in the VDWHRG model, Eq. (13) leads to the ideal HRG model. This method has been successfully applied to the GCE framework [27,44,45]. The pressure and the particle number density $n(T, \mu)$ of the van der Waals equation in the GCE is written as [45,49]

$$P(T,\mu) = P^{id}(T,\tilde{\mu}) - an^2(T,\mu)$$
 (14)

where $n(T, \mu)$ is the particle number density of the van der Waals gas, which is given by

$$n(T,\mu) = \frac{n^{id}(T,\tilde{\mu})}{1 + bn^{id}(T,\tilde{\mu})} \tag{15}$$

with P^{id} and n^{id} are the ideal gas pressure and particle number density, respectively. The reduced baryon chemical potential $(\tilde{\mu})$ is given by

$$\tilde{\mu} = \mu - bP(T, \mu) - abn^{2}(T, \mu) + 2an(T, \mu)$$
(16)

The energy density in this model is calculated as

$$\varepsilon = \frac{\varepsilon^{id}(T, \tilde{\mu})}{1 + bn^{id}(T, \tilde{\mu})} - an^2(T, \mu) \tag{17}$$

and the entropy density can be written as

$$s(T,\mu) = \frac{s^{id}(T,\tilde{\mu})}{1 + bn^{id}(T,\tilde{\mu})}$$
(18)

We assume that, for a hadronic system, the VDW interactions exist between all pair of baryons and between all pairs of antibaryons. The interaction between baryons-antibaryons, mesonsmesons and mesons-(anti)baryons are neglected. The pressure of VDWHRG model can be written as

$$P(T,\mu) = P_M(T,\mu) + P_B(T,\mu) + P_{\bar{R}}(T,\mu)$$
(19)

where pressure for mesons is given by

$$P_M(T,\mu) = \sum_{i \in M} P_j^{id}(T,\mu_j), \tag{20}$$

and the pressure for baryons and antibaryons are

$$P_B(T,\mu) = \sum_{j \in B} P_j^{id}(T, \tilde{\mu}_j^B) - an_B^2, \tag{21}$$

and

$$P_{\bar{B}}(T,\mu) = \sum_{i \in \bar{B}} P_j^{id}(T, \tilde{\mu}_j^{\bar{B}}) - an_{\bar{B}}^2, \tag{22}$$

where M, B, and \bar{B} represent mesons, baryons, and antibaryons, respectively. The modified chemical potential for (anti)baryons is given by

$$\tilde{\mu}_{j}^{B(\bar{B})} = \mu_{j} - bP_{B(\bar{B})} - abn_{B(\bar{B})}^{2} + 2an_{B(\bar{B})}, \tag{23}$$

where n_B and $n_{\bar{B}}$ refer to baryon and antibaryon number densities, respectively. Equation (16) has to be solved numerically to estimate the shifted chemical potential, $\tilde{\mu}$. The pressure as well as other thermodynamic quantities can be estimated after evaluating $\tilde{\mu}$. The total (anti)baryon number densities can be estimated by differentiating the $p_{B(\bar{B})}$ with respect to the baryochemical potential as:

$$n_{B(\bar{B})} = \frac{\sum_{j \in B(\bar{B})} n_j^{id}(T, \tilde{\mu}_j^{B(\bar{B})})}{1 + b \sum_{j \in B(\bar{B})} n_j^{id}(T, \tilde{\mu}_j^{B(\bar{B})})}.$$
 (24)

Further, the specific heat at constant volume (C_V) and the speed of sound squared (C_s^2) which is related to inverse of C_V are calculated as:

$$C_V = \left(\frac{\partial \varepsilon}{\partial T}\right)_V; \quad C_s^2 = \frac{\partial P}{\partial \varepsilon} = \frac{\partial P/\partial T}{\partial \varepsilon/\partial T} = \frac{s}{C_V}.$$
 (25)

The fluctuations of the conserved numbers are obtained from the derivative of the thermodynamic pressure with respect to the corresponding chemical potentials μ_B , μ_Q or μ_S . The *k*-th order generalized susceptibilities (χ) are written as;

$$\chi_k^X = \frac{d^k [P(T, \mu)/T^4]}{d(\mu_y/T)^k},\tag{26}$$

where X represents either B_i , Q_i , or S_i of the ith particle depending on whether the susceptibility χ^X represents net-baryon, net-electric charge or net-strangeness.

Experimentally measured particle number fluctuations are characterized by the central moments viz., $\langle (\delta N)^2 \rangle$, $\langle (\delta N)^3 \rangle$, and $\langle (\delta N)^4 \rangle$, where $\langle ... \rangle$ denotes the average over total number of events, N is the measured particle multiplicity, and $\delta N = N - \langle N \rangle$. Further, the central moments are related to the cumulants $(C_n, n = 1, 2, 3, 4)$ as follows: mean $M = C_1 = \langle N \rangle$; variance $\sigma^2 = C_2 = \langle (\delta N)^2 \rangle$; skewness $S = C_3/C_2^{3/2} = \langle (\delta N)^3 \rangle/\sigma^3$, and kurtosis $\kappa = C_4/C_2^2 = \langle (\delta N)^4 \rangle/\sigma^3 - 3$. The ratios of the cumulants are defined as the following combinations of the central moments, $\sigma^2/M = C_2/C_1$, $S\sigma = C_3/C_2$, and $\kappa\sigma^2 = C_4/C_2$. These ratios are well known volume-independent measures of particle number fluctuations. These ratios of moments/cumulants can be related to the susceptibilities of nth order (χ_n) obtained from lattice QCD or the HRG model calculations as $\sigma^2/M \sim \chi_{21} (= \chi_2/\chi_1)$, $S\sigma \sim \chi_{32} (= \chi_3/\chi_2)$, and $\kappa\sigma^2 \sim \chi_{42} (= \chi_4/\chi_2)$.

3. Results and discussions

Fig. 1 shows the binding energy per nucleon E_B/A as a function of nucleon number density at T=0 calculated using different versions of HRG models. The IHRG being the non-interacting model, hence shows no binding and the E_B/A values increase with n_B . The EVHRG and FLEVHRG models are having only the excluded volume term (*i.e.* repulsive interactions), hence

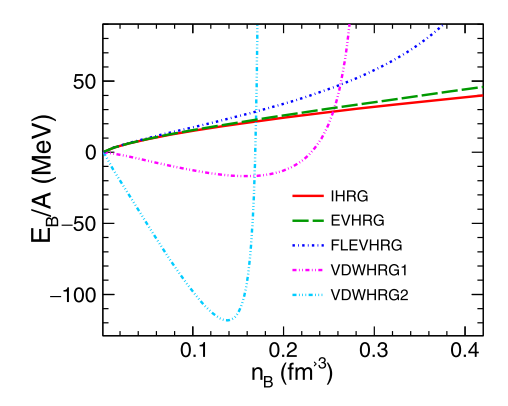


Fig. 1. The binding energy per nucleon (E_B/A) as a function of nucleon number density (n_B) calculated using different extended versions of HRG models at T=0.

 E_B is larger in these two models as compared to the IHRG model. The other two models (VD-WHRG1 and VDWHRG2) with van der Waals interactions show the negative values of E_B/A due to the inclusion of attractive interactions. As mentioned in Ref. [10], the values of VDW parameters a=329 MeV fm³ and b=3.42 fm³ in the VDWHRG1 model are extracted from the fit to the ground-state of the nuclear matter. Hence, this model reproduces the minimum $E_B/A \simeq -16$ MeV and $n_B \simeq 0.16$ fm⁻³ values. The other VDW based model VDWHRG2 [33] shows large negative E_B/A value because the VDW parameters a and b are extracted by minimizing χ^2 between VDW model and Lattice QCD data for thermodynamic parameters. The VDWHRG2 model gives large values of a=1250 MeV fm³ and b=5.747 fm³ as mentioned in Table 1.

Fig. 2 shows the temperature dependence of thermodynamic parameters like P/T^4 , ε/T^4 , s/T^3 , C_V/T^3 , $C_S^2 = \partial P/\partial \varepsilon$, and $(\varepsilon - 3p)/T^4$ at zero chemical potential $(\mu_B = \mu_Q = \mu_S = 1)$ 0) considering different cases of HRG such as IHRG, EVHRG, and VDWHRG models. The different HRG model results are compared with the lattice QCD results of the Hot-QCD Collaboration [3] and the Wuppertal-Budapest (WB) Collaboration [7] as shown in the same figure. The variation of P/T^4 with temperature is very small in all the considered models, indicating independent of the repulsive or attractive interaction between the hadrons. There is almost no effect of interaction till T = 150 MeV in thermodynamic parameters. The reason for this is that the effective degree of freedom of hadrons does not increase much up to this temperature and therefore correction due to excluded volume is small. Above T = 150 MeV, we find a substantial change in thermodynamic quantities. For higher temperatures the deviation is mostly dominated by baryons and also thermodynamic quantities are less sensitive to the mesonic radii [29]. Further, in the case of EVHRG, the suppression is more as compared to IHRG while considering the flavor dependent hard-core radius compared to fixed radii for mesons ($r_m = 0.2$ fm) and baryons $(r_b = 0.3 \text{ fm})$. It may be noted that baryon-baryon interaction has no effect at lower temperatures. At $\mu_B = 0$, the matter is dominated by mesons and their contribution is dominated over baryons. The behavior of the observables from the lattice QCD calculations at zero chemical potential is shown to be strongly correlated to the nuclear matter properties. The HRG model with higher binding energy can better describe the Lattice QCD data as compared to the other E-HRG models.

Figs. 3 show the energy dependence of susceptibility ratios ($\chi_{21} = \chi_2/\chi_1$, $\chi_{32} = \chi_3/\chi_2$, and $\chi_{42} = \chi_4/\chi_2$) for net-baryon (panels (a), (b), (c)), net-charge (panels (d), (e), (f)), and net-

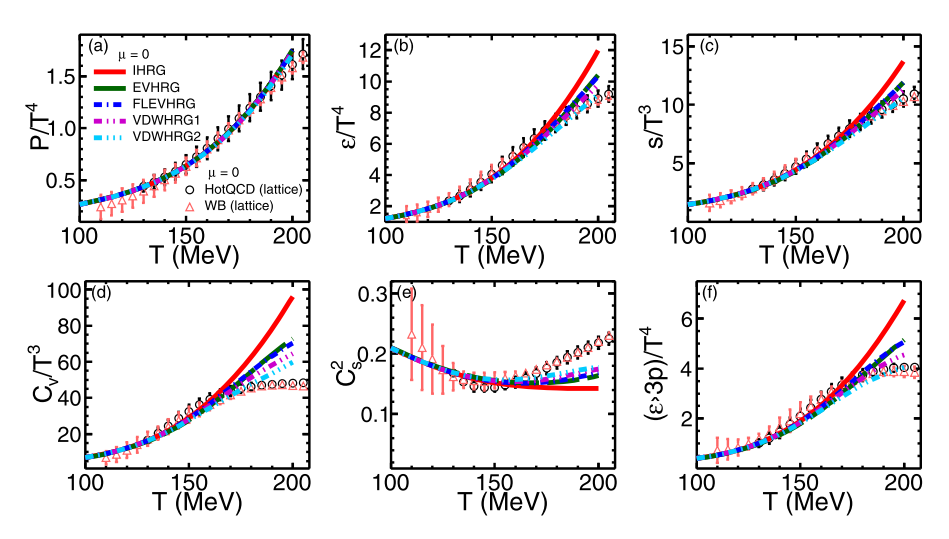


Fig. 2. The thermodynamic quantities P/T^4 , ε/T^4 , s/T^3 , C_V/T^3 , C_S^2 , and $(\varepsilon-3p)/T^4$ as a function of temperature at $\mu=0$ calculated using different HRG models. The open circle and triangle symbols are for HotQCD [3] and Wuppertal-Budapest (WB) [2] lattice data respectively. (For interpretation of the colors in the figure(s), the reader is referred to the web version of this article.)

strangeness (panels (g), (h)) by considering different cases of HRG model as listed in Table 1. The study has been carried out considering the full phase-space in transverse momentum (p_T) and pseudorapidity (η) . At lower energy, χ_{21}^B for net-baryon is close to unity and its value increases rapidly with increase of $\sqrt{s_{NN}}$. There is a small effect of interaction in the EVHRG and VDWHRG models. However, the results from these models are systematically lower compared to the IHRG model for all the studied energies. At low energy, the net-baryon χ_{32}^B is close to unity and its value decreases with increase of $\sqrt{s_{NN}}$. The estimated values of χ^B_{32} in both EVHRG and VDWHRG are lower than that of the IHRG model. Larger deviation from IHRG observed at lower collision energies, and all models give similar χ_{32}^B at higher $\sqrt{s_{NN}}$. For χ_{42}^B values from IHRG are close to Poisson expectation (which is at 1) for all energies. The values at lower energies are slightly lower than unity due to the correction of quantum statistics. In the EVHRG model, the χ_{42}^B values reduce to $\sim 10\%$ for lower energy ($\sqrt{s_{NN}} < 20 \text{ GeV}$) and approach to unity with the increase of energy while considering particle hard-core radii of 0.2 fm and 0.3 fm for mesons and baryons, respectively. The values are further reduced for lower energy with consideration of flavor dependent particle radii. With the inclusion of attractive interaction between the hadrons, χ_{42}^B strongly depends on $\sqrt{s_{NN}}$, indicating the suppression of particle number fluctuation in the VDW gas. The number density of proton increases with decrease in the beam energy which may be one of the reason for the increasing suppression in the EVHRG and VDWHRG models at lower collision energies [28].

The energy dependence of χ_{21}^Q , χ_{32}^Q , and χ_{42}^Q ratios for net-charge are shown in Fig. 3 (panels (d), (e), (f)). The χ_{21}^Q values increase rapidly with increasing $\sqrt{s_{NN}}$. The χ_{32}^Q values decrease with the increasing $\sqrt{s_{NN}}$ for all the cases of HRG. Similar to the χ_{32}^B for the net-baryon case, the χ_{32}^Q values in EVHRG and VDWHRG are lower as compared to results from the IHRG model. The deviation from the IHRG is larger at lower energies. The χ_{42}^Q for net-charge increases with energies and saturates at higher energies for all the cases of the HRG model. However,

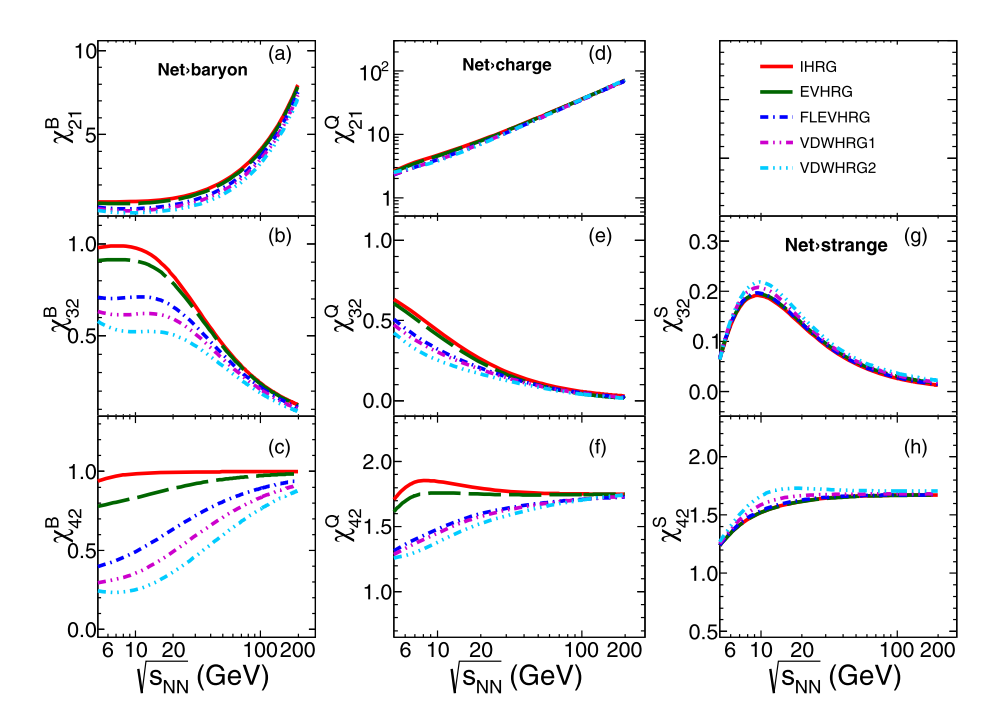


Fig. 3. The collision energy dependence of susceptibility ratios (χ_{21} , χ_{32} , and χ_{42}) for net-baryon (panels (a), (b), and (c)), net-charge (panels (d), (e), and (f)) and net-strangeness (panels (g) and (h)) calculated using different HRG models in full phase-space.

by including the repulsive and attractive interactions in the EVHRG and VDWHRG models, a larger deviation is observed from the IHRG. For all the cases, the decrease in χ_{42}^Q values at lower energies attribute to the effect of quantum statistics which is important for low mass hadrons such as pions and kaons.

Fig. 3 (panels (g), (h)) shows the energy dependence of χ_{32}^S and χ_{42}^S ratios for net-strangeness. It is to be noted that, χ_{21}^S diverges due to the imposed strangeness neutrality condition in the HRG model [46]. The value of χ_{32}^S increases with energy up to $\sqrt{s_{NN}} \simeq 10$ GeV and decreases thereafter. At lower energies, the results from FLEVHRG and VDWHRG2 are higher as compared to IHRG. At higher $\sqrt{s_{NN}}$, results from all the models are consistent. The χ_{42}^S value slowly increases with $\sqrt{s_{NN}}$ and saturates at higher energies. Hence, interactions between the particle have a small effect on the fluctuations of net-strangeness.

3.1. Acceptance effect on different models

Most of the experimental measurements are available for a limited fraction of the total phase-space due to finite detector acceptance. In an experiment we can detect only certain types of particle species due to inability of detectors to measure all them [47,55,56]. To compare the experimental measurements with model calculations, as well as the results from different experiments to each other, it is essential for the models to calculate the desired fluctuations within the same detector acceptance window. Here, we discuss the influence of different kinematic acceptance on cumulants of net conserved (baryon number, electric charge and strangeness) fluc-

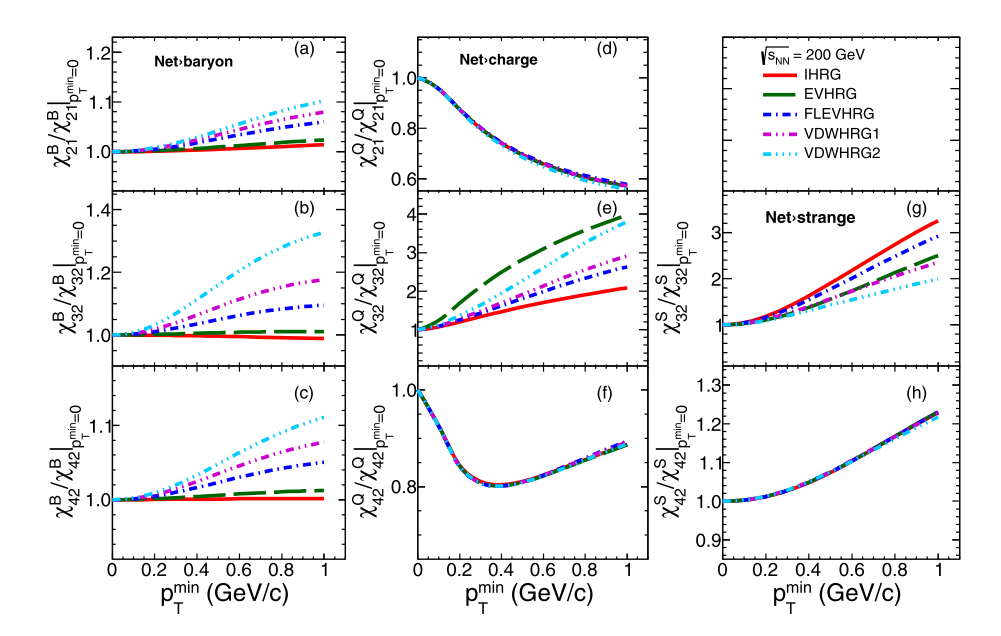


Fig. 4. The lower transverse momentum cut-off (p_T^{\min}) dependence of normalized susceptibility ratios $(\chi_{21}, \chi_{32}, \text{ and } \chi_{42})$ for net-baryon (panels (a), (b), and (c)), net-charge (panels (d), (e), and (f)) and net-strangeness (panels (g) and (h)) calculated for $\sqrt{s_{NN}}$ = 200 GeV using various E-HRG models. The maximum p_T has been set as 5.0 GeV/c and in full pseudo-rapidity.

tuations in different HRG models as mentioned in Sec. 2. The acceptance effects are studied by introducing the p_T and η cuts into the momentum integrals in Eqs. (3)–(6). We consider the effect of transverse momentum and pseudo-rapidity cuts on conserved number fluctuations in a static medium.

3.1.1. Effect of p_T -acceptance

Fig. 4 show the lower p_T cut-off dependence of susceptibility ratios normalized to the corresponding values with respect to full p_T acceptance for net-baryon (panels (a), (b), (c)), net-charge (panels (d), (e), (f)) and net-strangeness (panels (g), (h)) at $\sqrt{s_{NN}}$ = 200 GeV. In Fig. 4, the lower p_T cut-off has very minimal effect on the net-baryon fluctuations in both IHRG and EVHRG models. Similar observation were made for IHRG case in the previous study [47,55,56]. However, susceptibility ratios in the FLEVHRG and VDWHRG models have substantial dependence on the p_T^{min} cut-off. A maximum dependence occurs for the VDWHRG2 case where the van der Waals parameters are larger. The normalized susceptibility ratios of net-baryons increase with the lower side of the p_T cut-off. Fig. 4 (panels (d), (e), (f)) shows the normalized susceptibility ratios for net-charge fluctuations. The net-charge fluctuations are dominated by the contributions from pions, which are strongly influenced by the effects of quantum statistics. Therefore, the susceptibility ratios are strongly affected by the p_T^{\min} cut-off. Unlike the net-baryon case, there is no model dependence for the p_T^{min} cut-off on normalized χ_{21}^Q and χ_{42}^Q ratios. For a given p_T^{min} cut-off, the χ_{32}^Q values are different in various HRG models. Fig. 4 (panels (g), (h)) shows the normalized susceptibility ratios for net-strangeness fluctuations. The net-strangeness fluctuations are also strongly dependent on p_T^{\min} cut-off due to contributions from multi-strange states and quantum statistics effects of kaons. The χ_{32}^S ratios are dependent on the choice of the HRG models. There

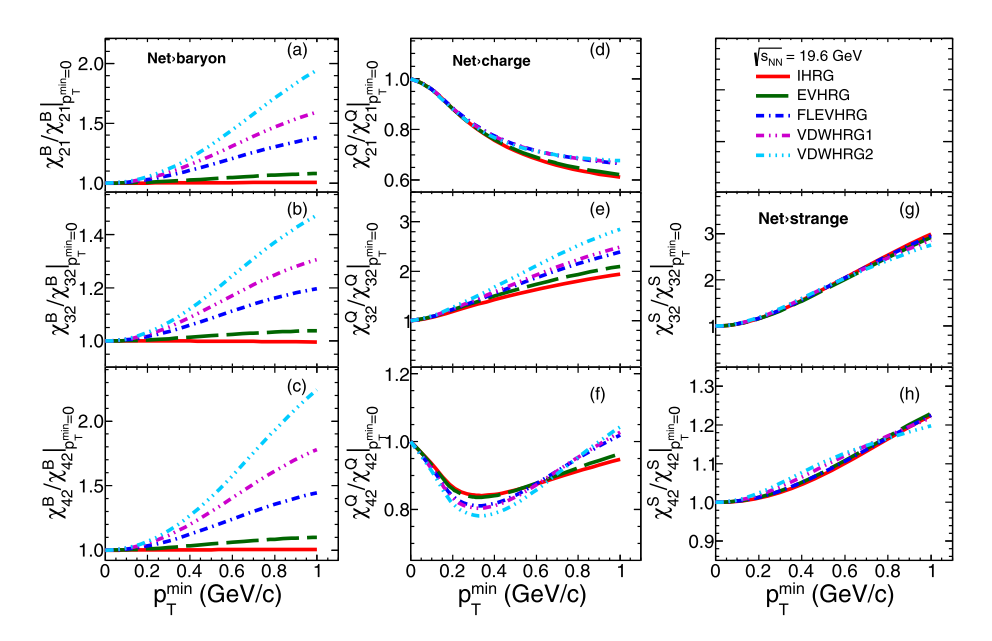


Fig. 5. The lower transverse momentum cut-off (p_T^{\min}) dependence of normalized susceptibility ratios $(\chi_{21}, \chi_{32}, \text{ and } \chi_{42})$ for net-baryon (panels (a), (b), and (c)), net-charge (panels (d), (e), and (f)) and net-strangeness (panels (g) and (h)) calculated for $\sqrt{s_{NN}}$ = 19.6 GeV using various E-HRG models. The maximum p_T has been set as 5.0 GeV/c and in full pseudo-rapidity.

is no model dependence on the normalized χ_{42}^S ratios for different p_T^{min} cut-off. Similar study has been performed at lower collision energy $\sqrt{s_{NN}} = 19.6$ GeV. Fig. 5 shows the normalized susceptibility ratios for net-baryon, net-charge and net-strangeness at $\sqrt{s_{NN}} = 19.6$ GeV. A stronger dependence of normalized susceptibility ratios observed for net-baryon fluctuations in different versions of HRG model. Similar p_T cut-off dependence observed for net-charge and net-strange fluctuations as in $\sqrt{s_{NN}} = 200$ GeV.

3.1.2. Effect of η -acceptance

Fig. 6 show the normalized susceptibility ratios as a function of the pseudo-rapidity cut ($|\Delta\eta|=2.5$) for net-baryon (panels (a), (b), (c)), net-charge (panels (d), (e), (f)), and net-strangeness (panels (g), (h)) using different HRG models at $\sqrt{s_{NN}}=200$ GeV. In Fig. 6 (panels (a), (b), (c)), the maximum η_{max} cut-off has no effect on the net-baryon fluctuations for the IHRG case. The susceptibility ratios show a strong dependence at the smaller $|\Delta\eta|$ window in both FLEVHRG and VDWHRG models. However, there is no dependence between models and $\Delta\eta$ cuts at higher $|\Delta\eta|>1.0$. Fig. 6 (panels (d), (e), (f)) show the normalized susceptibility ratios for net-charge fluctuations with different $\Delta\eta$ acceptance window. There is a strong dependence of $\Delta\eta$ cut in all the cases of HRG model for $|\Delta\eta|<1.0$. The normalized χ_{21}^Q and χ_{42}^Q show similar $\Delta\eta$ dependence in all the HRG models. The χ_{32}^Q values are different in various cases of HRG model. All the models show similar susceptibility ratios at higher $\Delta\eta$, i.e. $|\Delta\eta|>1.5$. Fig. 6 (panels (g), (h)) shows the normalized susceptibility ratios for net-strangeness fluctuations. The susceptibility ratios are strongly depend on $\Delta\eta$ cut particularly at lower windows and remain constant at higher $|\Delta\eta|>1.5$. The normalized χ_{32}^Q are similar for different HRG models, however the χ_{32}^S values are different for various HRG models. Further study has been carried out at lower collision energy,

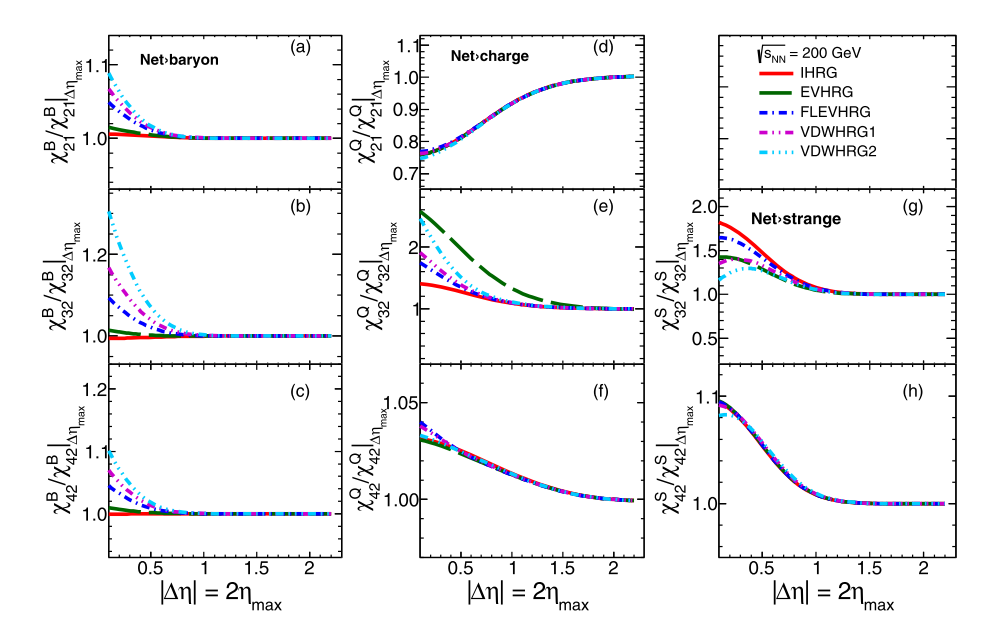


Fig. 6. The normalized susceptibility ratios (χ_{21} , χ_{32} , and χ_{42}) as a function of $\Delta\eta$ window for net-baryon (panels (a), (b), and (c)), net-charge (panels (d), (e), and (f)) and net-strangeness (panels (g) and (h)) calculated for $\sqrt{s_{NN}} = 200 \text{ GeV}$ using various E-HRG models in full p_T acceptance.

 $\sqrt{s_{NN}}$ = 19.6 GeV. Fig. 7 shows the normalized susceptibility ratios for net-baryon, net-charge and net-strangeness at $\sqrt{s_{NN}}$ = 19.6 GeV as a function of $\Delta\eta$. It is observed that at lower energy, normalized susceptibility ratios strongly depend on different HRG models for smaller $\Delta\eta$ as compared to $\sqrt{s_{NN}}$ = 200 GeV. It is also found that similar $\Delta\eta$ dependence for net-charge and net-strangeness fluctuations at lower energy as observed at higher energy, $\sqrt{s_{NN}}$ = 200 GeV.

3.2. Comparison with the experimental measurements

Experimentally measured moments $(M, \sigma, S, \text{ and } \kappa)$ of the net multiplicity distributions are related to the susceptibilities estimated from the model calculations (lattice QCD or HRG) as follows: $\sigma^2/M \sim \chi_2/\chi_1(=\chi_{21})$, $S\sigma \sim \chi_3/\chi_2(=\chi_{32})$, $\kappa\sigma^2 \sim \chi_4/\chi_2(=\chi_{42})$. In the following, different versions of the HRG model calculations are compared with the experimental results from STAR and PHENIX experiments measured in the central (0-5%) Au+Au collisions.

Fig. 8 shows the energy dependence of σ^2/M , $S\sigma$, and $\kappa\sigma^2$ of net-proton multiplicity distributions measured by the STAR experiment at RHIC [16] and [17]. The experimental data are measured within midrapidity (|y| < 0.5) with different transverse momentum range $0.4 \le p_T \le 0.8$ GeV/c (panels (a), (b), (c)) and $0.4 \le p_T \le 2.0$ GeV/c (panels (d), (e), (f)). Both the data sets show different absolute values of $S\sigma$ and $\kappa\sigma^2$ because of the different p_T acceptance. The statistical uncertainties are calculated using Delta theorem approach [57]. The experimental measurements are compared with the different versions of HRG models calculated within the same acceptance as the experiment. The difference between σ^2/M in the IHRG and different extensions of HRG model are negligible and all the models are consistent with the experimental data except at $\sqrt{s_{NN}} = 200$ GeV. For $S\sigma$ and $\kappa\sigma^2$, the results from the interaction models (EVHRG, FLEVHRG, and VDWHRG) are lower than IHRG, indicating the suppression of particle number

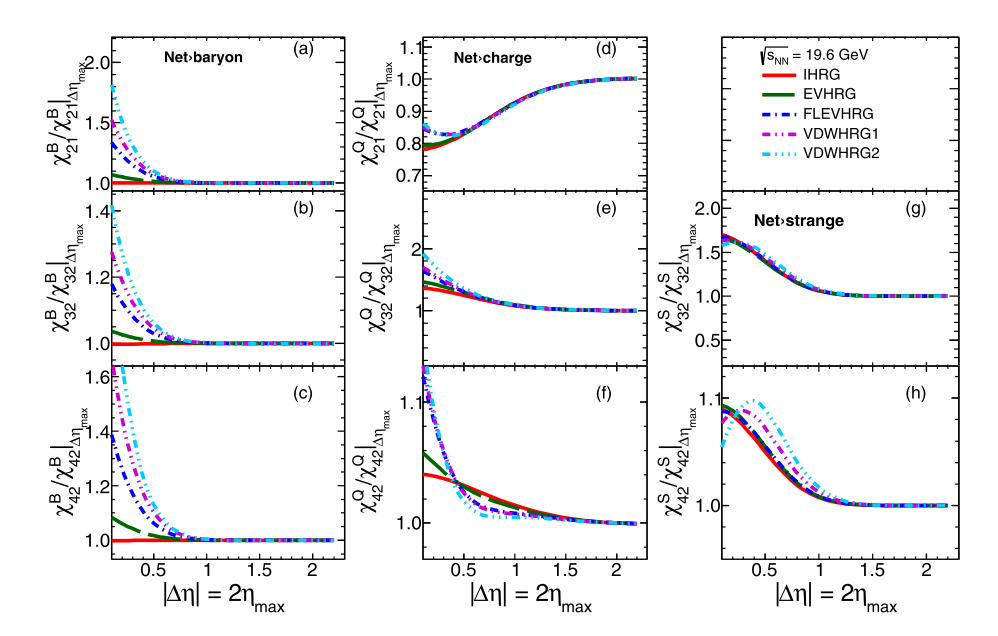


Fig. 7. The normalized susceptibility ratios (χ_{21} , χ_{32} , and χ_{42}) as a function of $\Delta\eta$ window for net-baryon (panels (a), (b), and (c)), net-charge (panels (d), (e), and (f)) and net-strangeness (panels (g) and (h)) calculated for $\sqrt{s_{NN}}$ = 19.6 GeV using various E-HRG models in full p_T acceptance.

fluctuation. The suppression increases at lower energies for the higher-order cumulants having flavor dependent hard-core radius and attractive interactions. At lower energies, the net-proton number density increases largely contributing to the net-baryon number fluctuations, which is one of the reasons for the increasing suppression in the VDW gas at lower RHIC energies [28]. The $\kappa\sigma^2$ values in the STAR data have a maximum deviation from the Poisson expectation at $\sqrt{s_{NN}}$ = 19.6 GeV and less suppression at lower energies, while the suppression in the FLEVHRG and VDWHRG models keep on increasing with the decreasing beam energies. The $S\sigma$ and $\kappa\sigma^2$ are strongly dependent on the types of interactions considered in the HRG calculations.

Fig. 9 shows the energy dependence of σ^2/M , $S\sigma$, and $\kappa\sigma^2$ of net-charge multiplicity distributions within $|\eta| < 0.5$ and a p_T range of 0.2 to 2.0 GeV/c measured by STAR experiment [18] and within $|\eta| < 0.35$ and p_T range of 0.3 and 2.0 GeV/c measured by PHENIX experiment [19] at RHIC. The statistical errors are calculated using Delta theorem method [57]. Here, we would like to briefly discuss about the statistical error calculations in both the STAR and PHENIX experiments. The statistical errors on $S\sigma$ and $\kappa\sigma^2$ are correlated and are dependent on both variance (σ) of the multiplicity distribution, detector efficiency and the number of events. As mentioned in [57], the statistical errors are more dependent on σ than the number of events. Hence, experiments having wider multiplicity distribution will have larger errors on $S\sigma$ and $\kappa\sigma^2$. Since STAR experiment has larger acceptance compared to PHENIX, it contributes to larger statistical error on the higher moments. Further, STAR net-charge distributions have larger σ compared to net-proton distributions, which contributes to the larger statistical error in the net-charge results than the net-proton results, although the number of analyzed events are similar.

The experimental net-charge fluctuation results are compared with the different HRG model calculations by considering the corresponding kinematic acceptance cuts. In case of STAR net-charge fluctuation results (panels (a), (b), (c)), σ^2/M values from all the considered HRG models

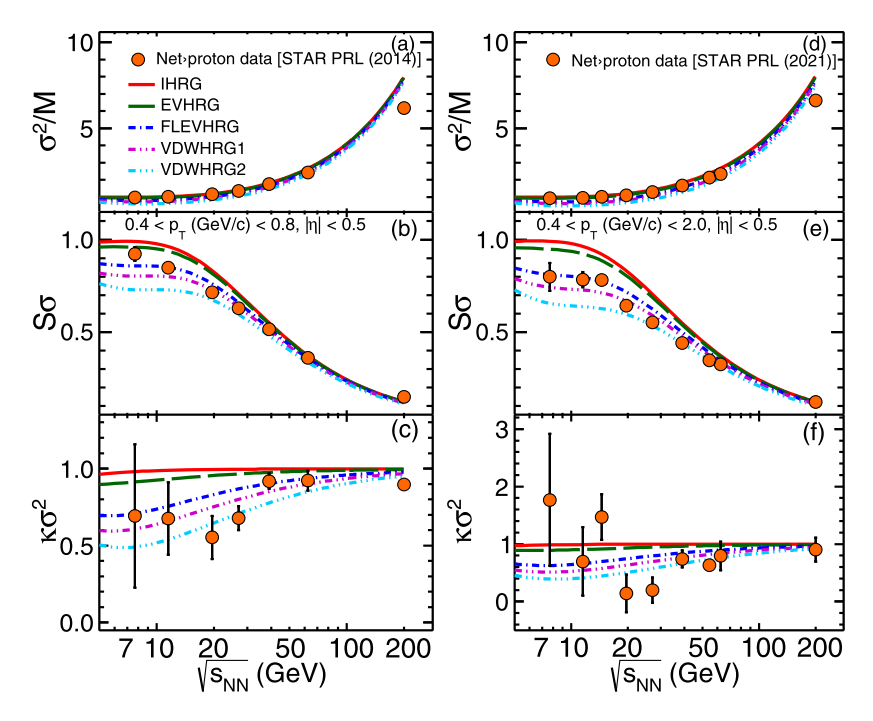


Fig. 8. The collision energy dependence of $\sigma^2/M(\sim \chi_{21})$, $S\sigma(\sim \chi_{32})$, and $\kappa\sigma^2(\sim \chi_{42})$ for net-baryon calculated using various E-HRG models within the experimental acceptance. The model calculations are compared with the experimental net-proton cumulant ratios for the most central (0%–5%) Au+Au collisions measured by the STAR experiment with different momentum acceptance [16,17].

are systematically lower than the experimental data at all energies. However, there is a small dependence between the choice of HRG models. The $S\sigma$ values have larger suppression at lower $\sqrt{s_{NN}}$. The $S\sigma$ and $\kappa\sigma^2$ values from the experimental data are explained by all cases of HRG models because of large uncertainties in the measured STAR experimental data. In case of PHENIX net-charge fluctuation results (panels (d), (e), (f)), σ^2/M values from the experimental data closely follow the model calculations. On the other hand, the calculated values of $S\sigma$ considering IHRG and EVHRG models fail to explain the experimental data. The discrepancy between the experimental data and the model calculations reduces with the inclusion of flavor dependent hard-core radius and attractive interactions in the HRG model. The $\kappa\sigma^2$ values are reasonably explained by different HRG model calculations except for the case of VDWHRG2, which shows a decreasing trend at lower energies. At higher energies, all the models show similar results.

In most of the experiments all the baryons are not detected, hence the net-baryon number fluctuations are not measured directly in the experiment. The net-baryon fluctuations are accessible via measuring the net-proton distributions. The net-charge fluctuations are accessible by measuring the stable charged particles such as pions, kaons, and protons along with their antiparticles. Similarly, the measurement of net-kaon fluctuations acts as a proxy for net-strangeness fluctuations, because higher mass strange particles are not directly measured. The difference between net-strangeness and net-kaon, as well as between net-baryon and net-proton, using IHRG model has been discussed in [47]. Fig. 10 shows the energy dependence of $S\sigma$, and $\kappa\sigma^2$ of net-kaon multiplicity distributions for central (0%–5%) Au+Aucollisions within $|\eta| < 0.5$ and p_T range

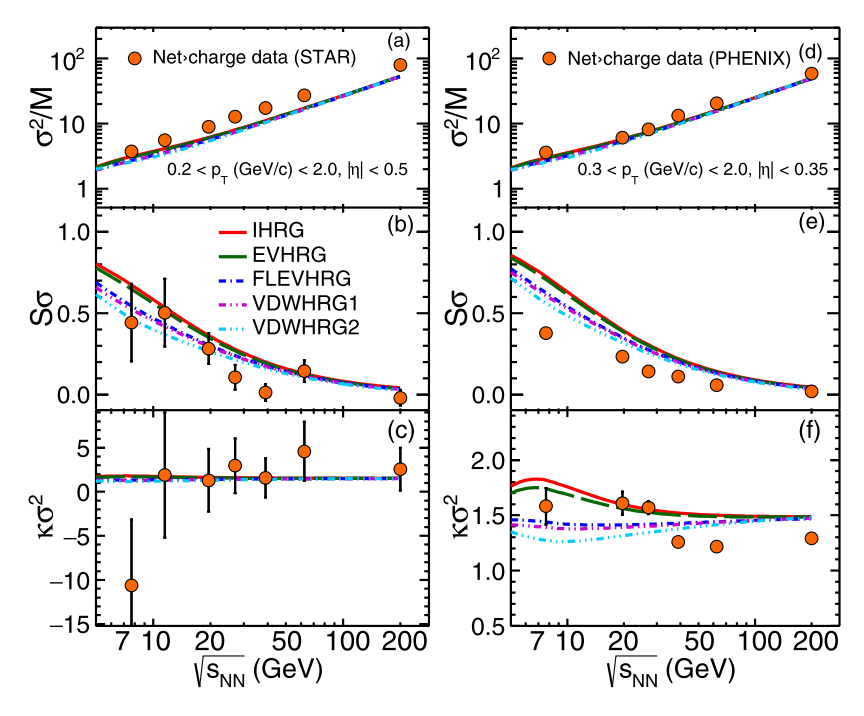


Fig. 9. The collision energy dependence of $\sigma^2/M(\sim \chi_{21})$, $S\sigma(\sim \chi_{32})$, and $\kappa\sigma^2(\sim \chi_{42})$ for net-electric charge calculated using various E-HRG models within the experimental acceptance. The model calculations are compared with the experimental net-charge cumulant ratios for the most central (0%-5%) Au+Aucollisions measured by the STAR (panels (a), (b), and (c)) [18] and PHENIX (panels (d), (e), and (f)) [19] experiments.

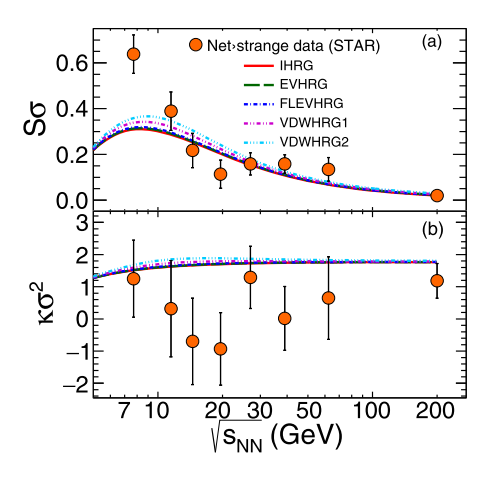


Fig. 10. The collision energy dependence of $S\sigma(\sim\chi_{32})$ and $\kappa\sigma^2(\sim\chi_{42})$ for net-strangeness calculated using various E-HRG models within the experimental acceptance. The model calculations are compared with the experimental net-kaon cumulant ratios for the most central (0%–5%) Au+Aucollisions measured by the STAR experiment [20].

within 0.2 to 1.6 GeV/c measured by STAR experiment [20]. The experimental measurements are compared with the HRG model calculations without and with including interactions. The

experimental data on χ_{32}^S are well explained by all the considered model calculations except at $\sqrt{s_{NN}}$ = 7.7 GeV. There is a small difference while considering various choices of interactions. The HRG model calculations for $\kappa\sigma^2$ are above the experimental measurements. Unlike the net-baryon case, a small difference in χ_{42}^S values are observed while considering different HRG models.

4. Summary

We have studied the fluctuations of conserved numbers using different interactions in the HRG model to understand the strongly interacting matter at high temperature and baryon density. This study will help to understand the phase diagram of quantum chromodynamics (QCD) at non-zero temperature and baryon chemical potential. For this, we have studied the effect of different interactions in the HRG model by estimating various thermodynamic parameters such as P/T^4 , ϵ/T^4 , s/T^3 , C_V/T^3 , C_s^2 and $(\epsilon-3p)/T^4$ at $\mu=0$. It is found that P/T^4 has a small dependence on the interactions that included in the HRG model. Other thermodynamic quantities viz., ϵ/T^4 , s/T^3 , C_s^2 and C_V/T^3 are independent of the choice of the interactions at lower T, however, they start deviating from the ideal HRG values for T > 150 MeV. The susceptibility ratios (χ_{21} , χ_{32} , and χ_{42}) of net-baryon, net-electric charge and net-strangeness are estimated as a function of $\sqrt{s_{NN}}$ considering different HRG models at full phase-space and also within the experimental acceptance. The χ_{32} and χ_{42} ratios of net-baryon as a function of $\sqrt{s_{NN}}$ show large variations between different E-HRG models. Further, the impact of p_T^{min} cut-off as well as $\Delta \eta$ windows on the normalized susceptibilities ratios are studied. It is found that p_T^{min} cut-off has a negligible effect on net-baryon fluctuations calculated using the IHRG model. On the other hand, the results from EVHRG and VDWHRG models show a strong dependence on p_T^{min} cutoff. There is a strong dependence on p_T^{min} cut-off observed in the normalized χ_{32} and χ_{42} ratios for net-charge and net-strangeness with the inclusion of different interactions in the HRG model. The normalized susceptibility ratios show a strong dependence on $\Delta \eta$ at its lower values while employing EVHRG and VDWHRG models. The χ_{32} ratios for net-charge and net-strangeness show a strong dependence on $\Delta \eta$ window and also with different interactions included in the HRG model. Hence, it is important to consider the proper kinematic acceptance while comparing the experimental measurement with the model calculations. As shown in this work, the extended versions of the HRG model are very sensitive to kinematic acceptance even, particularly for net-proton results. Further, the EVHRG and VDWHRG calculations are compared with the experimental measurements for fluctuations of net-proton, net-charge, and net-kaon multiplicity distributions. There is a strong model dependence on the net-baryon results for $S\sigma$ and $\kappa\sigma^2$ values, particularly at lower collision energies. The repulsive and attractive interactions lead to larger suppression for higher-order cumulants at larger VDW parameters and lower beam energies. The net-charge fluctuations show larger models dependence at lower energies for both STAR and PHENIX acceptance. However, all the different models show similar results at higher energies. This study will be helpful to understand the fluctuation measurements in the experimental data with different interactions in the HRG model.

CRediT authorship contribution statement

S.P. Behera: Data generating and software writing and editing, Original draft preparation, Conceptualization.

D.K. Mishra: Data plotting, software writing and draft reviewing and editing, Conceptualization.

Declaration of competing interest

The authors declare that they have no known competing financial interests or personal relationships that could have appeared to influence the work reported in this paper.

Acknowledgements

We would like to acknowledge A. K. Mohanty, S. Samanta and P. Garg for the stimulating discussion related to this work.

References

- [1] M.A. Stephanov, K. Rajagopal, E.V. Shuryak, Phys. Rev. Lett. 81 (1998) 4816.
- [2] S. Borsanyi, Z. Fodor, C. Hoelbling, S.D. Katz, S. Krieg, K.K. Szabo, Phys. Lett. B 730 (2014) 99.
- [3] A. Bazavov, et al., HotQCD Collaboration, Phys. Rev. D 90 (2014) 094503.
- [4] M.A. Stephanov, Prog. Theor. Phys. Suppl. 153 (2004) 139, Int. J. Mod. Phys. A 20 (2005) 4387.
- [5] A. Bazavov, et al., Phys. Rev. Lett. 109 (2012) 192302.
- [6] S. Ejiri, F. Karsch, K. Redlich, Phys. Lett. B 633 (2006) 275.
- [7] Z. Fodor, S.D. Katz, J. High Energy Phys. 0404 (2004) 050.
- [8] M.A. Stephanov, K. Rajagopal, E.V. Shuryak, Phys. Rev. D 60 (1999) 114028.
- [9] F. Karsch, Acta Phys. Pol. Suppl. 7 (2014) 117.
- [10] V. Vovchenko, M.I. Gorenstein, H. Stoecker, Phys. Rev. Lett. 118 (2017) 182301.
- [11] A. Bazavov, et al., Phys. Rev. Lett. 111 (2013) 082301.
- [12] V. Koch, A. Majumder, J. Randrup, Phys. Rev. Lett. 95 (2005) 182301.
- [13] M. Asakawa, U.W. Heinz, B. Muller, Phys. Rev. Lett. 85 (2000) 2072.
- [14] M. Asakawa, S. Ejiri, M. Kitazawa, Phys. Rev. Lett. 103 (2009) 262301.
- [15] M.M. Aggarwal, et al., STAR Collaboration, Phys. Rev. Lett. 105 (2010) 022302.
- [16] L. Adamczyk, et al., STAR Collaboration, Phys. Rev. Lett. 112 (2014) 032302.
- [17] J. Adam, et al., STAR Collaboration, Phys. Rev. Lett. 126 (2021) 092301.
- [18] L. Adamczyk, et al., STAR Collaboration, Phys. Rev. Lett. 113 (2014) 092301.
- [19] A. Adare, et al., PHENIX Collaboration, Phys. Rev. C 93 (2016) 011901.
- [20] L. Adamczyk, et al., STAR, Phys. Lett. B 785 (2018) 551.
- [21] P. Braun-Munzinger, K. Redlich, J. Stachel, in: R.C. Hwa, et al. (Eds.), Quark Gluon Plasma, vol. 3, 2004, pp. 491–599.
- [22] J. Cleymans, H. Oeschler, K. Redlich, S. Wheaton, Phys. Rev. C 73 (2006) 034905.
- [23] A. Andronic, P. Braun-Munzinger, K. Redlich, J. Stachel, J. Phys. G 38 (2011) 124081.
- [24] R. Hagedorn, J. Rafelski, Phys. Lett. B 97 (1980) 136.
- [25] G.D. Yen, M.I. Gorenstein, W. Greiner, S.N. Yang, Phys. Rev. C 56 (1997) 2210.
- [26] A. Andronic, P. Braun-Munzinger, J. Stachel, M. Winn, Phys. Lett. B 718 (2012) 80.
- [27] D.H. Rischke, M.I. Gorenstein, H. Stoecker, W. Greiner, Z. Phys. C 51 (1991) 485.
- [28] J. Fu, Phys. Lett. B 722 (2013) 144.
- [29] A. Bhattacharyya, S. Das, S.K. Ghosh, R. Ray, S. Samanta, Phys. Rev. C 90 (2014) 034909.
- [30] V. Vovchenko, D.V. Anchishkin, M.I. Gorenstein, Phys. Rev. C 91 (2015) 024905.
- [31] V.V. Begun, M. Gazdzicki, M.I. Gorenstein, Phys. Rev. C 88 (2013) 024902.
- [32] S. Sahoo, D.K. Mishra, P.K. Sahu, Nucl. Phys. A 1018 (2022) 122362.
- [33] S. Samanta, B. Mohanty, Phys. Rev. C 97 (2018) 015201.
- [34] S.R. Amendolia, et al., Phys. Lett. B 178 (1986) 435.
- [35] T. Udem, A. Huber, B. Gross, J. Reichert, M. Prevedelli, M. Weitz, T.W. Hansch, Phys. Rev. Lett. 79 (1997) 2646.
- [36] P. Mergell, U.G. Meissner, D. Drechsel, Nucl. Phys. A 596 (1996) 367.
- [37] B. Povh, J. Hufner, Phys. Rev. Lett. 58 (1987) 1612.

- [38] P. Braun-Munzinger, I. Heppe, J. Stachel, Phys. Lett. B 465 (1999) 15.
- [39] P. Alba, V. Vovchenko, M.I. Gorenstein, H. Stoecker, Nucl. Phys. A 974 (2018) 22.
- [40] V. Vovchenko, H. Stoecker, J. Phys. G 44 (2017) 055103.
- [41] V. Vovchenko, H. Stoecker, Phys. Rev. C 95 (2017) 044904.
- [42] K. Werner, I. Karpenko, T. Pierog, M. Bleicher, K. Mikhailov, Phys. Rev. C 82 (2010) 044904.
- [43] A.V. Merdeev, L.M. Satarov, I.N. Mishustin, Phys. Rev. C 84 (2011) 014907.
- [44] V. Vovchenko, D.V. Anchishkin, M.I. Gorenstein, J. Phys. A 48 (2015) 305001.
- [45] V. Vovchenko, D.V. Anchishkin, M.I. Gorenstein, Phys. Rev. C 91 (2015) 064314.
- [46] F. Karsch, K. Redlich, Phys. Lett. B 695 (2011) 136.
- [47] P. Garg, D.K. Mishra, P.K. Netrakanti, B. Mohanty, A.K. Mohanty, B.K. Singh, N. Xu, Phys. Lett. B 726 (2013) 691.
- [48] A. Bzdak, V. Koch, V. Skokov, Phys. Rev. C 87 (2013) 014901.
- [49] V. Vovchenko, D.V. Anchishkin, M.I. Gorenstein, R.V. Poberezhnyuk, Phys. Rev. C 92 (2015) 054901.
- [50] R. Dashen, S.K. Ma, H.J. Bernstein, Phys. Rev. 187 (1969) 345.
- [51] V. Vovchenko, L. Jiang, M.I. Gorenstein, H. Stoecker, Phys. Rev. C 98 (2018) 024910.
- [52] D.K. Mishra, P. Garg, P.K. Netrakanti, A.K. Mohanty, Phys. Rev. C 94 (2016) 014905.
- [53] M. Albright, J. Kapusta, C. Young, Phys. Rev. C 90 (2014) 024915.
- [54] V. Koch, Chapter of the book "Relativistic Heavy Ion Physics", in: R. Stock (Ed.), Landolt-Boernstein New Series I, vol. 23, Springer, Heidelberg, 2010, pp. 626–652.
- [55] F. Karsch, K. Morita, K. Redlich, Phys. Rev. C 93 (2016) 034907.
- [56] B. Ling, M.A. Stephanov, Phys. Rev. C 93 (2016) 034915.
- [57] X. Luo, J. Phys. G 39 (2012) 025008.